11th World Congress on Computational Mechanics (WCCM XI)
5th European Conference on Computational Mechanics (ECCM V)
6th European Conference on Computational Fluid Dynamics (ECFD VI)
E. Oñate, J. Oliver and A. Huerta (Eds)

TRANSITIONAL FLOW SIMULATION IN TURBOMACHINERY WITH A HIGH-ORDER ACCURATE METHOD

MARCO LORINI*, ANTONIO GHIDONI*, FRANCESCO BASSI†, ALESSANDRO COLOMBO† AND STEFANO REBAY*

* Department of Mechanical and Industrial Engineering
University of Brescia
via Branze 38, 25123 Brescia, Italy
e-mail: marco.lorini@ing.unibs.it, antonio.ghidoni@ing.unibs.it, stefano.rebay@ing.unibs.it

†Department of Industrial Engineering
University of Bergamo
viale Marconi 5, 24044 Dalmine, Italy
e-mail: francesco.bassi@unibg.it, alessandro.colombo@unibg.it

Key words: RANS Equations, DG Method, Transition Modeling, Intermittency, Multi-mode Model.

Abstract. Various methods have been proposed in the finite volume context to predict the laminar-turbulent transition, but, according to the literature, not yet in the high-order context. We considered the transition model proposed by Kožulović and Lapworth (2009), which is integral, non-local and based upon experimental correlations. All the relevant modes of transition were taken into account. We implemented this model into a high-order accurate discontinuous Galerkin (DG) method with implicit time integration to solve the RANS equations coupled with the $k-\omega$ turbulence model. The model was applied to two test cases, namely the flat plate (T3A configuration) and the T106A turbine cascade. Results obtained with and without transition model were compared with experimental data. The transition model seems to be a necessary feature to predict correctly these flow fields.

1 INTRODUCTION

Nowadays numerical simulations have become an important tool in almost all sectors of fluids engineering. Computational fluid dynamics (CFD) has been widely accepted as one of the main methods to evaluate the performances of the new turbomachinery designs. Industrial CFD applications range from classical single- and multi-blade row simulations

in steady and unsteady mode, to cavity flows, heat transfer and combustion chamber simulations.

Due to the increasing required level of resolution and to analyze ever more complex geometries and flows, there is a growing concern that state-of-the-art Finite Volume (FV) technology requires, and will continue to require, too expensive computational resources. The demand for high resolution naturally leads to consider methods with a higher order of accuracy, such as discontinuous Galerkin (DG) methods [1]. The DG method is one of the most promising techniques in this respect because of its robustness, accuracy and flexibility. DG methods are in fact finite element methods which account for the physics of wave propagation by means of Riemann solvers as in upwind FV methods but, unlike the latter, can achieve higher-order accuracy on general unstructured grids using high degree polynomials as in the classical (continuous) finite element method.

In spite of the recent advances in scale-resolving CFD simulations, the most commonly considered equations to simulate turbulent flows in industrial applications are the Reynolds-Averaged Navier-Stokes (RANS) equations. Due to their lower computational cost, RANS equations, supplemented by a suitable partial differential turbulence model, can represent a reasonable compromise between accuracy and expense. These turbulence models are very well suited for high Reynolds number flows, whereas for low Reynolds numbers flows (as in low pressure gas-turbines), where a large part of the boundary layer is laminar or transitional, they can provide wrong results. In fact the boundary layer development, the losses, the efficiency and the heat transfer are greatly affected by the location and the extent of the laminar-to-turbulent transition. Therefore, the ability to accurately predict the transition is crucial for the design of efficient and reliable machines.

The MIGALE code, based on the DG spatial discretization, has been already used to study the transitional flow through the T106A turbine cascade [2], with the low-Reynolds version of the k-ω turbulence model. In this work we extended the prediction capabilities of the code coupling the turbulence model with an integral and non-local transition model developed in the context of the finite volume (FV) methods [3] and based on the empirical correlation proposed by Abu-Ghannam and Shaw [4]. The transition model was validated computing the flow over a flat plate and through a turbine cascade

2 GOVERNING EQUATIONS

The governing equations can be written as:

$$\frac{\partial \rho}{\partial t} + \frac{\partial}{\partial x_j}(\rho u_j) = 0, \tag{1}$$

$$\frac{\partial}{\partial t}(\rho u_i) + \frac{\partial}{\partial x_j}(\rho u_j u_i) = -\frac{\partial p}{\partial x_i} + \frac{\partial \widehat{\tau}_{ji}}{\partial x_j}, \tag{2}$$

$$\frac{\partial}{\partial t}(\rho e_0) + \frac{\partial}{\partial x_j}(\rho u_j h_0) = \frac{\partial}{\partial x_j}\left[u_i \widehat{\tau}_{ij} - q_j\right] - \tau_{ij}\frac{\partial u_i}{\partial x_j} + \beta^* \rho \overline{k} e^{\widetilde{\omega}}, \tag{3}$$

$$\frac{\partial}{\partial t}(\rho k) + \frac{\partial}{\partial x_j}(\rho u_j k) = \frac{\partial}{\partial x_j}\left[(\mu + \sigma^* \overline{\mu}_t)\frac{\partial k}{\partial x_j}\right] + \tau_{ij}\frac{\partial u_i}{\partial x_j} - \beta^* \rho \overline{k} e^{\widetilde{\omega}} \tag{4}$$

$$\begin{aligned}\frac{\partial}{\partial t}(\rho\widetilde{\omega}) + \frac{\partial}{\partial x_j}(\rho u_j \widetilde{\omega}) &= \frac{\partial}{\partial x_j}\left[(\mu + \sigma\overline{\mu}_t)\frac{\partial \widetilde{\omega}}{\partial x_j}\right] + \alpha\frac{\tau_{ij}}{\overline{k}}\frac{\partial u_i}{\partial x_j} - \beta\rho e^{\widetilde{\omega}} \\ &\quad + (\mu + \sigma\overline{\mu}_t)\frac{\partial \widetilde{\omega}}{\partial x_k}\frac{\partial \widetilde{\omega}}{\partial x_k} + \sigma_d \frac{\rho}{e^{\widetilde{\omega}}}\max\left(\frac{\partial k}{\partial x_k}\frac{\partial \widetilde{\omega}}{\partial x_k}; 0\right)\end{aligned} \tag{5}$$

where the pressure, the total stress tensor, the heat flux vector, and the limited value of turbulent kinetic energy $\overline{k}$ are defined as

$$p = (\gamma - 1)\rho\left(e_0 - u_k u_k/2\right), \qquad \widehat{\tau}_{ij} = 2\mu S_{ij} + \tau_{ij}, \tag{6}$$

$$q_j = -\left(\frac{\mu}{\mathrm{Pr}} + \frac{\overline{\mu}_t}{\mathrm{Pr}_t}\right)\frac{\partial h}{\partial x_j}, \tag{7}$$

$$\overline{k} = \max\left(0, k\right). \tag{8}$$

Here γ is the ratio of gas specific heats, Pr and Pr_t are the molecular and turbulent Prandtl numbers and S_{ij} and Ω_{ij} are the mean strain-rate and the rate-of-rotation tensors. The closure coefficients α, α^*, β, β^*, σ, σ^*, σ_d are those of the low-Reynolds number k-ω model of Wilcox [5]. Notice that Eq. (5) of the k-ω turbulence model is not in standard form since the variable $\widetilde{\omega} = \log\omega$ is used, see [6].

2.1 DG space discretization

The governing equations can be written in compact form as

$$\frac{\partial \mathbf{q}}{\partial t} + \boldsymbol{\nabla}\cdot\mathbf{F}_c(\mathbf{q}) + \boldsymbol{\nabla}\cdot\mathbf{F}_v(\mathbf{q}, \boldsymbol{\nabla}\mathbf{q}) + \mathbf{s}(\mathbf{q}, \boldsymbol{\nabla}\mathbf{q}) = \mathbf{0}, \tag{9}$$

where $\mathbf{q} \in \mathbb{R}^m$ denotes the vector of the m primitive variables, $\mathbf{s} \in \mathbb{R}^m$ the source term, d the space dimension, $\mathbf{F}_c, \mathbf{F}_v \in \mathbb{R}^M \otimes \mathbb{R}^N$ the inviscid and viscous flux functions.

A weak formulation of Eq. (9) is obtained multiplying each scalar law by an arbitrary smooth test function $v_j \in \mathbf{v}$, $1 \leq j \leq m$, and integrating by parts:

$$\begin{aligned}\int_\Omega v_j \frac{\partial q_j}{\partial t}\,\mathrm{d}\mathbf{x} - \int_\Omega \boldsymbol{\nabla} v_j \cdot \mathbf{F}_j(\mathbf{q}, \boldsymbol{\nabla}\mathbf{q})\,\mathrm{d}\mathbf{x} \\ + \int_{\partial\Omega} v_j \mathbf{F}_j(\mathbf{q}, \boldsymbol{\nabla}\mathbf{q})\cdot\mathbf{n}\,\mathrm{d}\sigma + \int_\Omega v_j \mathbf{s}_j(\mathbf{q}, \boldsymbol{\nabla}\mathbf{q})\,\mathrm{d}\mathbf{x} = 0,\end{aligned} \tag{10}$$

where $\mathbf{F}_j$ is the sum of the inviscid and viscous flux vectors, Ω the computational domain, $\partial\Omega$ the boundary of Ω, $\mathbf{n}$ the unit normal vector to the boundary.

Let Ω_h be an approximation of the domain $\Omega \in \mathbb{R}^d$, $\mathcal{T}_h = \{K\}$ a mesh of Ω_h, i.e. a collection of "finite elements" K, $\mathcal{F}_h = \{F\}$ the mesh faces, and let $\mathbf{V}_h$ denotes a discontinuous finite element space spanned by polynomial functions continuous only inside each element K, i.e.

$$\mathbf{V}_h \stackrel{\text{def}}{=} \left[\mathbb{P}_d^l\left(\mathcal{T}_h\right)\right]^m, \tag{11}$$

where

$$\mathbb{P}_d^l \stackrel{\text{def}}{=} \{v_h \in L^2(\Omega_h) : v_h|_K \in \mathbb{P}_d^l, \forall K \in \mathcal{T}_h\} \tag{12}$$

is the space of polynomials of degree at most l on the element K. Hierarchical and orthogonal shape functions are adopted and are obtained using a modified Gram-Schmidt procedure, assuming as a starting point a set of monomial functions [7]. The solution $\mathbf{q}$, the test function $\mathbf{v}$ are replaced with finite element approximations $\mathbf{q}_h$ and $\mathbf{v}_h$, belonging to the space $\mathbf{V}_h$. The DG formulation of the problem (10) requires to find $\mathbf{q}_h \in \mathbf{V}_h$ such that

$$\begin{aligned}\sum_{K\in\mathcal{T}_h}\int_K v_{h,j}\frac{\partial q_{h,j}}{\partial t}\,\mathrm{d}\mathbf{x} - \sum_{K\in\mathcal{T}_h}\int_K \boldsymbol{\nabla}_h v_{h,j}\cdot\mathbf{F}_j\left(\mathbf{q}_h, \boldsymbol{\nabla}_h\mathbf{q}_h + \mathbf{r}(\llbracket\mathbf{q}_h\rrbracket)\right)\,\mathrm{d}\mathbf{x} \\ + \sum_{F\in\mathcal{F}_h}\int_F \llbracket v_{h,j}\rrbracket\cdot\widehat{\mathbf{f}}_j\left(\mathbf{q}_h^{\pm}, \left(\boldsymbol{\nabla}_h\mathbf{q}_h + \eta_F\mathbf{r}_F(\llbracket\mathbf{q}_h\rrbracket)\right)^{\pm}\right)\,\mathrm{d}\sigma \\ + \sum_{K\in\mathcal{T}_h}\int_K v_{h,j}\mathbf{s}_j\left(\mathbf{q}_h, \boldsymbol{\nabla}_h\mathbf{q}_h + \mathbf{r}(\llbracket\mathbf{q}_h\rrbracket)\right)\,\mathrm{d}\mathbf{x} = \mathbf{0} \\ \mathbf{v}_h \in \mathbf{V}_h,\end{aligned} \tag{13}$$

where $\mathbf{r}$ and $\mathbf{r}_F$ are the global and the local lifting operators, η_F a stability parameter, and $\widehat{\mathbf{f}}$ is the sum of the inviscid and the viscous numerical fluxes.

The numerical flux function $\widehat{\mathbf{f}}$, appearing in the boundary integral of Eq. (13), is introduced in order to uniquely define the flux at the elements interfaces, to obtain a consistent and conservative approximation of Eq. (10), and to prescribe the boundary data. The flux $\widehat{\mathbf{f}}$ is the sum of an inviscid, $\widehat{\mathbf{f}}_c$, and a viscous, $\widehat{\mathbf{f}}_v$, part. The former is based on the Godunov flux computed with an exact Riemann solver. For the latter the BR2 scheme, proposed in [8] and theoretically analyzed in [9, 10], is employed.

2.2 Transition model

All the relevant modes of the transition are taken into account by this model, *i.e.* the natural/bypass mode and the separation induced mode. Each transition mode yields an intermittency value, namely γ_{NB} and γ_{SI}, and the maximum value is applied to the source terms of the turbulence model. In particular Eqs. (4) and (5) are rewritten as:

$$\frac{\partial}{\partial t}(\rho k) + \frac{\partial}{\partial x_j}(\rho u_j k) = \gamma_P \tau_{ij}\frac{\partial u_i}{\partial x_j} - \gamma_D\beta^*\rho\overline{k}e^{\tilde{\omega}_r} + \frac{\partial}{\partial x_j}\left[(\mu + \sigma^*\overline{\mu}_t)\frac{\partial k}{\partial x_j}\right], \tag{14}$$

$$\frac{\partial}{\partial t}(\rho\tilde{\omega}) + \frac{\partial}{\partial x_j}(\rho u_j\tilde{\omega}) = \gamma_P\frac{\alpha}{\overline{\overline{k}}}\tau_{ij}\frac{\partial u_i}{\partial x_j} - \gamma_D\beta\rho e^{\tilde{\omega}_r} + (\mu+\sigma\overline{\mu}_t)\frac{\partial\tilde{\omega}}{\partial x_k}\frac{\partial\tilde{\omega}}{\partial x_k} + \frac{\partial}{\partial x_j}\left[(\mu+\sigma\overline{\mu}_t)\frac{\partial\tilde{\omega}}{\partial x_j}\right] , \tag{15}$$

where:

$$\gamma_P = \max(\gamma_{NB};\gamma_{SI}) ,$$
$$\gamma_D = \max(\min(\gamma_P;1.0);0.02) .$$

In particular, an intermittency value $\gamma = 0$ corresponds to a laminar boundary layer, while $\gamma = 1$ to a fully turbulent boundary layer. The intermittency in the free-stream region is set to one.

2.2.1 Natural and bypass mode

Since the disturbance amplification process that leads to the natural and bypass transition is a continuous mechanism, these modes are modelled by one correlation. Both the boundary layer edge and the integral values of the boundary layer are required. As proposed by Abu-Ghannam and Shaw [4], transition onset is determined by evaluating a momentum thickness Reynolds number, $Re_{\theta,S}$, at which transition begins. In the model proposed by Kožulović and Lapworth [3] the correlation is:

$$Re_{\theta,S} = \left[1045\cdot\exp\left(-\frac{Tu_E[\%]}{1\%}\right)\right] + f_p + 155 , \tag{16}$$

where

$$f_p = 220\cdot\exp\left(-\frac{Tu_E[\%]}{0.9\%}\right)\cdot\left[\arctan\left(\frac{\lambda_\theta}{0.02}+0.842\right) - 0.7\right] , \tag{17}$$

and

$$\lambda_\theta = \min\left[\frac{\theta^2}{\nu_E}\frac{\partial U_E}{\partial s}, \frac{0.058\left(H_{12}-4.0\right)^2}{H_{12}-1.0} - 0.068\right] , \tag{18}$$

where the subscript $_E$ represents the quantities at the edge of the boundary layer, Tu_E the turbulence intensity, ν_E the kinematic viscosity, θ the momentum thickness, U_E the

velocity along the edge of the boundary layer, $H_{12} = \delta/\theta$, δ the displacement thickness, and s the streamline direction.

In a similar vein a momentum thickness Reynolds number at the end of transition is computed:

$$Re_{\theta,E} = Re_{\theta,S} \cdot \left\{ 1.6 + \left[1.3 \cdot \exp\left(-\frac{Tu_E[\%]}{2\%} \right) \right] \right\} . \tag{19}$$

The intermittency, γ_{NB} is determined comparing the limit values with the local momentum thickness Reynolds number, Re_θ:

$$Re_\theta = \frac{U_E \theta}{\nu_E} . \tag{20}$$

$$\begin{aligned} &\text{If } Re_\theta < Re_{\theta,S} && \Rightarrow \ \gamma_{NB} = 0 && \text{laminar flow ,} \\ &\text{if } Re_\theta > Re_{\theta,E} && \Rightarrow \ \gamma_{NB} = 1 && \text{turbulent flow ,} \\ &\text{if } Re_{\theta,S} < Re_\theta < Re_{\theta,E} && \Rightarrow \ \gamma_{NB} = 1 - \exp\left(-5 \cdot \varphi^{1.2}\right) && \text{transitional flow ,} \end{aligned} \tag{21}$$

where:

$$\varphi = \frac{Re_\theta - Re_{\theta,S}}{Re_{\theta,E} - Re_{\theta,S}} . \tag{22}$$

2.2.2 Separation induced mode

For this transition mode, we chose to implement the previous version of the model, as reported in [11]. In case of a separation induced transition, the model allows an extra intermittency between the separation onset and the reattachment point. In this way it's possible to have intermittency values greater than 1, when needed. The separation region is characterized by negative wall shear stress, τ_w. To compute the intermittency for this transition mode, γ_{SI}, the model requires first a preliminary intermittency, γ_{vl}:

$$\gamma_{vl} = \min\left(f_{Re} \cdot f_H \cdot f_{Tu}; 3\right) + \min\left(f_\lambda; 2\right) , \tag{23}$$

where:

$$f_{Re} = \max\left[\frac{4}{\pi} \cdot \arctan\left(\frac{Re_\theta - 100}{200} \right); 0.25 \right] , \tag{24}$$

$$f_H = \max\left[\frac{16}{\pi} \cdot \arctan\left(\frac{H_{12} - 1.4}{2.6} \right); 0.25 \right] , \tag{25}$$

$$f_{Tu} = \max\left[\frac{2}{\pi}\cdot\arctan\left(\frac{Tu_E[\%]}{1\%}\right); 0.35\right], \tag{26}$$

$$f_{\lambda} = \frac{1}{2}\max\left(-\lambda_\theta - 0.1; 0\right)\cdot\left[1 + 2\cdot\exp\left(-0.4\cdot\frac{Tu_E[\%]}{1\%}\right)\right]. \tag{27}$$

The computation of the intermittency γ_{SI}, as shown in Eq. 28, requires the preliminary intermittency of the upstream line, γ_{up}, as well as the distance from the upstream line, Δs_{up}.

$$\begin{aligned} &\text{if } \gamma_{vl} > \gamma_{up}: \qquad \gamma_{SI} = \min\left[\gamma_{vl}, \gamma_{up} + \left(8\cdot\frac{\Delta s_{up}}{l}\right)\right], \\ &\text{if } \gamma_{vl} < \gamma_{up}: \qquad \gamma_{SI} = \max\left[\gamma_{vl}, \gamma_{up} - \left(10\cdot\frac{\Delta s_{up}}{l}\right)\right]. \end{aligned} \tag{28}$$

3 RESULTS

We validated and assessed the transition model in the computation of two test cases: the compressible turbulent flow over a flate plate (test T3A of the ERCOFTAC SIG 10) and through the T106A turbine cascade for different Reynolds numbers [12].

3.1 Flat plate (T3A)

We first validated the transition model for a simple zero-pressure gradient flat plate. In particular the T3A test case of the ERCOFTAC was used, characterized by the conditions reported in Tab. 1. We compared the prediction of the transition onset and transition length with the available experimental data [13]. A mesh with 3264 linear quadrilateral elements was used (available at `http://turbmodels.larc.nasa.gov`). We assigned at the inlet section the conditions proposed by Cutrone *et al.* [14], provided in Tab. 2.

Table 1: ERCOFTAC T3A test case.

	T3A test case
Upstream Velocity (m/s)	5.4
Upstream Tu (%)	3.0
Pressure Gradient	Zero

Table 2: Inlet conditions for the T3A test case.

	T3A test case
Tu_{in} (%)	10
$(\mu_T/\mu)_{in}$	0.35

The predicted skin friction coefficient for a $\mathbb{P}^3$ solution approximation is shown in Fig. 1, where the result of a fully turbulent simulation is also depicted. The model is in good agreement with the experimental data and significantly increased the prediction capabilities of the k-ω turbulence model as shown by the results obtained with a fully turbulent simulation. Figure 1 shows that the transition onset is delayed and the transition

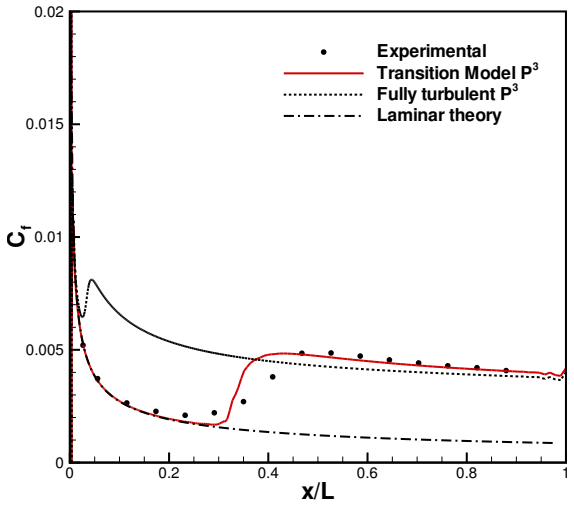

Figure 1: Distribution of the skin friction coefficient for the T3A flat plate case, $\mathbb{P}^3$ approximation.

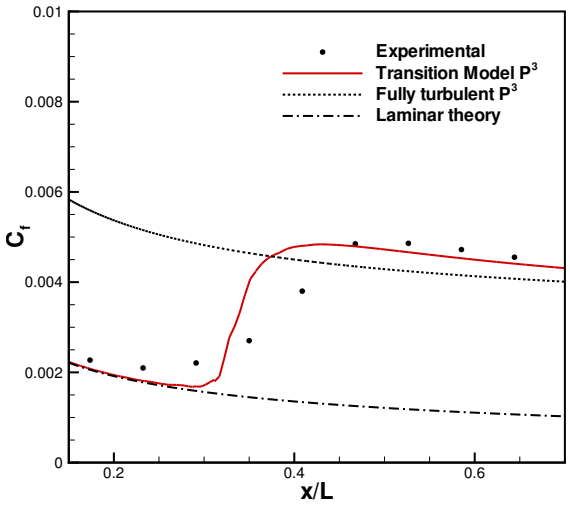

Figure 2: Detail of the transition region for the T3A flat plate case, $\mathbb{P}^3$ approximation.

region is too short. On the other hand the transition end is predicted at the right position. This behaviour has been reported also by Cutrone *et al.* [14] for other intermittency-based transition models.

3.2 Turbine cascade (T106A)

For the second test case the T106A turbine cascade was considered, which is characterized by challenging transitional flow conditions. It is a low-pressure turbine cascade designed by MTU Aero Engines, which has been extensively investigated in experimental and computational studies [12, 2].

We ran all the computations in parallel up to a $\mathbb{P}^3$ solution approximation, initializing the $\mathbb{P}^0$ solution from the uniform flow at the outflow conditions and the higher-order solutions from the lower order ones. Adiabatic wall boundary condition was imposed on blade surface. At the inflow, the total temperature, total pressure, flow angle $\alpha_1 = 37.7°$, and turbulence intensity $Tu_1 = 4\%$ were prescribed. At the outflow, the static pressure was set, resulting in a downstream isentropic Mach number, $M_{2,is} = 0.59$. In order to evaluate the transition model for both bypass and separation-induced transition, we chose two different values of the Reynolds number based on the downstream isentropic conditions and on the blade chord, $Re = 1.5 \times 10^5$ and $Re = 1.1 \times 10^6$. All computations have been performed by using a grid composed of 4268 quadratic quadrilateral elements.

3.2.1 Natural and bypass transition

The first test was carried out with a Reynolds number, $Re_{2,is} = 1.1 \times 10^6$. In fact, the flow separation is not present for this condition and we verified the correct prediction of

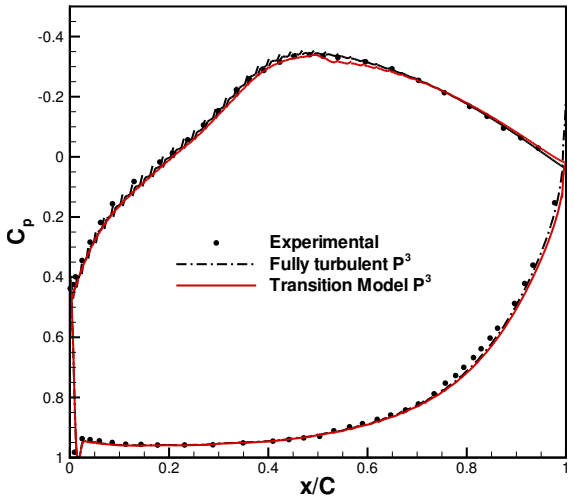

Figure 3: Distribution of the pressure coefficient for the T106A ($Re_{2,is} = 1.1 \times 10^6$) test case, $\mathbb{P}^3$ approximation.

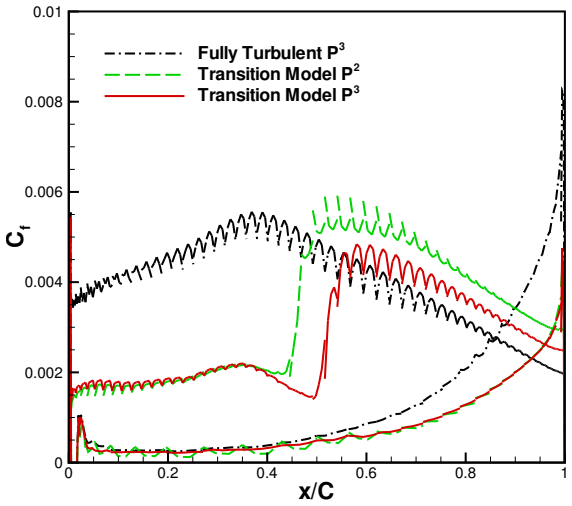

Figure 4: Distribution of the skin friction coefficient for the T106A ($Re_{2,is} = 1.1 \times 10^6$) test case, $\mathbb{P}^2$ and $\mathbb{P}^3$ approximation.

the natural and bypass transition mode.

In Fig. 3 we present the C_p distribution along the blade for the $\mathbb{P}^3$ approximation. On the pressure side the curve is in good agreement with the experimental data, whereas on suction side there is a little difference at $x/C \simeq 0.5$, where transition begins.

Fig. 4 shows the C_f distribution along the blade for all the polynomial approximations. The transition location moved downstream increasing the polynomial order of the approximation. The correct location was predicted by the $\mathbb{P}^3$ approximation. The oscillations on the suction side show a lack of resolution in the boundary layer. In fact the size of the elements adjacent to the wall in the direction normal to the wall is equal to $y^+ \approx 1$ for a Reynolds number $Re = 0.15 \times 10^6$, but it is probably too high for $Re = 1.1 \times 10^6$.

In Tab. 3 we report the loss coefficient, ζ. As expected, it was overestimated by the fully turbulent computation, while the transition model allowed to predict almost the correct value for the $\mathbb{P}^3$ approximation.

Table 3: Loss coefficient, ζ, for the T106A test case.

	$\mathbb{P}^1$	$\mathbb{P}^2$	$\mathbb{P}^3$	fully turbulent $\mathbb{P}^3$	Experimental
$Re_{2,is} = 1.1 \times 10^6$	0.0327	0.0227	0.0201	0.0269	0.02
$Re_{2,is} = 0.15 \times 10^6$	0.0368	0.0353	0.0329	0.0398	0.032

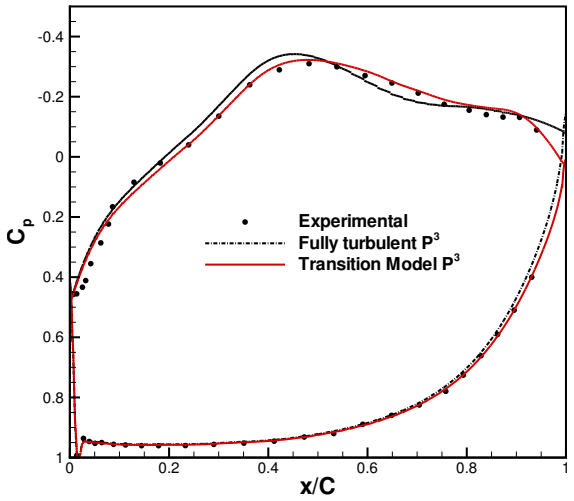

Figure 5: Distribution of the pressure coefficient for the T106A ($Re_{2,is} = 0.15 \times 10^6$) test case, $\mathbb{P}^3$ approximation.

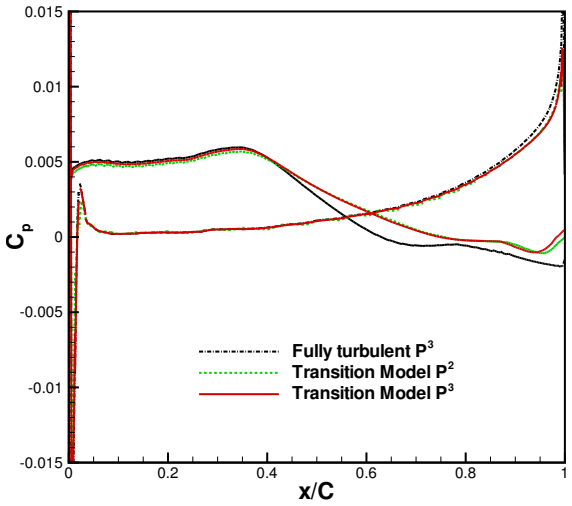

Figure 6: Distribution of the skin friction coefficient for the T106A ($Re_{2,is} = 0.15 \times 10^6$) test case, $\mathbb{P}^2$ and $\mathbb{P}^3$ approximation.

3.2.2 Separation induced transition

In the second test the Reynolds number was set to 0.15×10^6 to see how the model handled a recirculating flow. The experimental data available for the above mentioned flow conditions is the distribution of pressure coefficient, C_p, along the blade, as reported in [12]. On the suction side, the peak value of C_p is located at about 47% of the chord. A separation bubble is evident over the rear portion of the suction surface with the separation at 70% of the chord. A pressure plateau, typically associated with the shear layer of a steady separation bubble extends to 90% of the chord. At this location, pressure recovery begins as the separated shear layer undergoes transition and reattaches as turbulent boundary layer by 96% of the chord. On the pressure side the boundary layer is completely attached.

Fig. 5 shows the C_p distribution along the blade for $\mathbb{P}^3$ approximation. On the pressure side the curve is in perfect agreement with the experimental data. On the suction side the model approximates reasonably well the experimental results and in particular captures the pressure plateau and the reattachment point near the trailing edge (characterized by positive values of C_p), whereas the fully turbulent computation does not.

In Fig. 6 we present the C_f distribution over the entire blade. The C_f curve associated with the $\mathbb{P}^3$ approximation becomes negative near $x/C = 0.73$, putting in evidence the detachment of the flow, which reattaches at $x/C = 0.97$, when C_f becomes again positive. The $\mathbb{P}^2$ curve becomes negative near $x/C = 0.73$, in correspondence of the flow separation, but delays the reattachment at $x/C = 1$. The C_f curve associated with the fully turbulent computation predicts the detachment of the flow at approximately $x/C = 0.65$, but without reattachment.

As reported in Tab. 3, again the loss coefficient, ζ, was overestimated by the fully turbulent computation. The transition model allowed to predict for the $\mathbb{P}^3$ approximation a value closer to the experimental.

4 CONCLUSIONS

The non-local transition model of Kožulović and Lapworth has been implemented into a high-order accurate discontinuous Galerkin method for the simulation of compressible flows. We validated the model on two test cases, namely the flat plate (T3A configuration) and the T106A turbine cascade in two different configurations.

The model led to significant improvements with respect to the fully turbulent computations. The results were in quite good agreement with the experimental data for all the configurations.

The empirical nature of the model reduced the computational resources required but limited its general applicability. However, the model significantly increased the performances of the numerical code in the test cases mentioned above and seems to be a necessary feature to predict correctly transitional flow fields.

REFERENCES

[1] F. Bassi, L. Botti, A. Colombo, A. Ghidoni and S. Rebay. Discontinuous Galerkin for turbulent flows. In: Z. J. Wang. *Adaptive High-Order Methods in Computational Fluid Dynamics*. World Scientific Publishing, Iowa State University, USA, 2011.

[2] A. Ghidoni, A. Colombo, S. Rebay and F. Bassi. Simulation of the transitional flow in a low pressure gas turbine cascade with a high-order discontinuous Galerkin method. *Journal of Fluids Engineering*, Vol. **135**(7), Paper No. 071101, 2013.

[3] D. Kožulović and B. L. Lapworth. An approach for inclusion of a non-local transition model in a parallel unstructured computational fluid dynamics code. *Journal of Turbomachinery*, Vol. **131**(3). Paper No. 031008, 2009.

[4] B. J. Abu-Ghannam and R. Shaw. Natural transition of boundary layers – The effects of turbulence, pressure gradient, and flow history. *Journal Mechanical Engineering Science*, Vol. **22**(5), 213–228, 1980.

[5] D. C. Wilcox. Turbulence Modelling for CFD. *DCW industries Inc.*, La Cañada, CA 91011, USA, 1993.

[6] F. Bassi, A. Crivellini, S. Rebay and M. Savini. Discontinuous Galerkin Solution of the Reynolds-Averaged Navier-Stokes and k-ω turbulence model equations. *Comput. & Fluids*, Vol. **34**, 507–540, 2005.

[7] F. Bassi, L. Botti, A. Colombo, D. A. Di Pietro and P. Tesini. On the flexibility of agglomeration based physical space discontinuous Galerkin discretizations. *Journal of Computational Physics*, Vol. **231**, 45–65, 2012.

[8] F. Bassi, S. Rebay, G. Mariotti, S. Pedinotti and M. Savini. A high-order accurate discontinuous finite element method for inviscid and viscous turbomachinery flows. In: R. Decuypere and G. Dibelius. *Proceedings of the 2nd European Conference on Turbomachinery Fluid Dynamics and Thermodynamics*, Technologisch Instituut, Antwerpen, Belgium, 99–108, 1997.

[9] F. Brezzi, G. Manzini, D. Marini, P. Pietra and A. Russo. Discontinuous Galerkin approximations for elliptic problems. *Numer. Methods Partial Differential Equations*, Vol. **16**, 365–378, 2000.

[10] D. N. Arnold, F. Brezzi, B. Cockburn and D. Marini. Unified analysis of discontinuous Galerkin methods for elliptic problems. *SIAM J. Numer. Anal.*, Vol. **39**, 1749–1779, 2002.

[11] D. Kožulović. Modellierung des Grenzschichtumschlags bei Turbomaschinenströmungen unter Berücksichtigung mehrerer Umschlagsarten. *PhD Thesis für Ruhr-Universität Bochum*, 2007.

[12] H. Hoheisel. Entwicklung neuer Entwurfskonzepte für zwei Turbinengitter, Teil III, Ergebnisse T106. *Tech. rep., Institut für Entwurfsaerodynamik*, Braunschweig, 1981.

[13] J. Coupland. ERCOFTAC Special interest group on laminar to turbulent transition and retransition: T3A and T3B test cases. 1990.

[14] L. Cutrone, P. De Palma, G. Pascazio and M. Napolitano. An evaluation of bypass transition models for turbomachinery flows. *International Journal of Heat and Fluid Flow*, Vol. **28**, 161–177, 2007.